Standing spin waves in perpendicularly magnetized triangular dots

Julia Kharlan,[1,2] Pavlo Bondarenko,[1] Maciej Krawczyk,[3] Olga Salyuk,[1,2] Elena Tartakovskaya,[1] Aleksandra Trzaskowska,[3] and Vladimir Golub[1]

[1]*Institute of Magnetism, National Academy of Sciences of Ukraine, 36b Vernadsky blvd, 03142 Kiev, Ukraine*

[2]*National Technical University of Ukraine "Igor Sikorsky Kyiv Polytechnic Institute," 37 Peremogy ave, 03056 Kyiv, Ukraine*

[3]*Faculty of Physics, Adam Mickiewicz University in Poznan, Umultowska 85, 61–614 Poznan, Poland*

(Received 15 July 2019; published 21 November 2019)

Standing spin waves in triangular dots (truncated pyramids) were investigated both experimentally and theoretically. Arrays of nickel triangular pyramids with the base side of 270 nm and height of 70 nm were deposited on Si (111) substrate. The spectra of ferromagnetic resonance were obtained at room temperature with an external saturating magnetic field directed perpendicular to the array plane. The theoretical approach, which allows to describe standing spin wave modes both in perpendicular magnetized regular prisms and in close to prisms truncated pyramids, was developed. Theoretically calculated resonance fields for the observed modes are in a good correlation with the experiment.

DOI: 10.1103/PhysRevB.100.184416

I. INTRODUCTION

Study of ferromagnetic confined objects (nanoparticles) and their arrays is of great interest during the last decades due to the possibility of their applications for magnetic random access memory (MRAM), biometric probes, magnetic logic devices, etc. [1–3]. Investigation of magnetic dynamics of such structures is mainly focused on the study of standing spin waves (SW) modes in isolated elements or propagating SW in arrays of interacting nanoparticles, which are actually the basis of magnonics [4–6]. Spectra of these waves are mainly determined by nanoparticles shape.

Standing SWs in thin saturated cylindrical dots [7–11], rectangular dots [12], and microrings [13,14] were studied both experimentally and theoretically. The investigations of magnetic properties of triangular elements were mostly focused on the experimental study and computer simulation of the vortex magnetic structures. The problems of the formation and manipulation of magnetic vortices [15,16], their chirality and polarity [17], vortex dynamics [18,19], and resonant properties of vortex core [20] were considered. There were several attempts to simulate magnetic dynamics of triangular dots in vortex, Y, and buckle states [21–23]. However, at present moment, there are neither experimental results on magnetic dynamics of triangular dots in saturated state nor analytical theory, like that was developed for cylindrical and square dots. Such investigation is an actual problem because the anisotropy of magnetic properties of triangular particles results in the diversity of SW modes and possibility to increase information recording density.

Here we present the experimental observation of standing SW modes in triangular dots in the external saturating magnetic field directed perpendicular to their base plane. An analytical approach to describe the magnetic dynamics both in the regular triangular prisms and truncated pyramids has been developed.

II. EXPERIMENT

The samples for the experiments were made using the well-developed method of nanosphere lithography [24]. The process of production was realized in three stages. During the first stage the Si (111) substrate surface was covered with a monolayer of PS-latex beads. The size of the sample was $1 \times 1\,\mathrm{cm}^2$, the diameter of beads was 570 nm. During the second stage nickel was deposited on the substrates using electron beam evaporation technique. Ni atoms penetrate between the beads and forming islands of about $h = 70\,\mathrm{nm}$ height on Si surface (see Fig. 1). Then the monolayer of PS-latex beads was removed from the surface immersing the samples in tetra-hydrofurane for 15 minutes. Detailed description of the sample preparation can be found in Refs. [24,25]. Topography of the samples was investigated at room temperature using the atomic force microscopy (AFM) operating in the contact mode. The size of the mapped area was $3\,\mu\mathrm{m} \times 3\,\mu\mathrm{m}$. Atomic force microscopy (AFM) investigation (Fig. 1) showed that the shape of nickel islands was close to truncated regular triangular pyramid (frustrum) with the base side $a = 270\,\mathrm{nm}$. The supposition that the islands are of triangular shape was used in the theoretical model presented here.

Standard electron spin resonance spectrometer Bruker ELEXSYS E500 operating at 9.86 GHz was used to record ferromagnetic resonance spectra at room temperature. The external magnetic field was applied perpendicularly to the array plane. Four practically equidistant resonance peaks were observed in the experiment (Fig. 2). The distance between them is of about 500 Oe. Such type of spectrum is quite similar to that was observed in thin disklike ferromagnetic dots [7], where the dipolar eigenmodes naturally (circular membrane oscillations) have a shape of a zeroth-order Bessel function resulting in practically equidistant resonance peaks position.

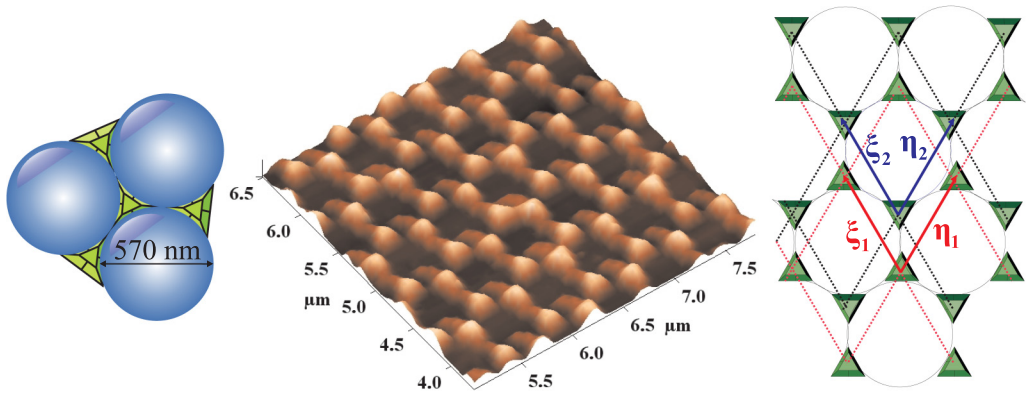

FIG. 1. A schematic presentation of a formation of the triangular dots array using the nanosphere lithography method (left). AFM image of the periodic array of nickel islands used in the experiments (middle). A schematic presentation of the triangular dots array (right). The hexagonal array is formed by nested regular triangular lattices with basis vectors $\boldsymbol{\zeta}_1$, $\boldsymbol{\eta}_1$ and $\boldsymbol{\zeta}_2$, $\boldsymbol{\eta}_2$.

III. THEORETICAL MODEL

The theory of SW spectrum has been developed approximating shape of nickel islands by regular triangular prism and truncated pyramid (with the base side a and height h, see Fig. 3). Preliminary analysis using standard fiction magnetic charge method has shown that magnetostatic interaction between perpendicularly magnetized dots is quite small: the mean magnetostatic field produced by other dots is of about 130 Oe for triangular prisms and even less for truncated pyramids array. This value is much less than the variation of demagnetizing fields inside dots and will be disregarded during the following theoretical analysis. Besides, in perpendicularly magnetized dot arrays the interdot dipole-dipole interaction creates an additional effective perpendicular bias field, which practically does not change the structure of the spectrum of spin wave modes [7]. It can be introduced into analysis of the experimental spectra by slight modification of perpendicular anisotropy value. The resonance magnetic field value for all observed resonance modes is large enough to align the mean magnetization in the field direction and the magnetization value is close to the saturation magnetization.

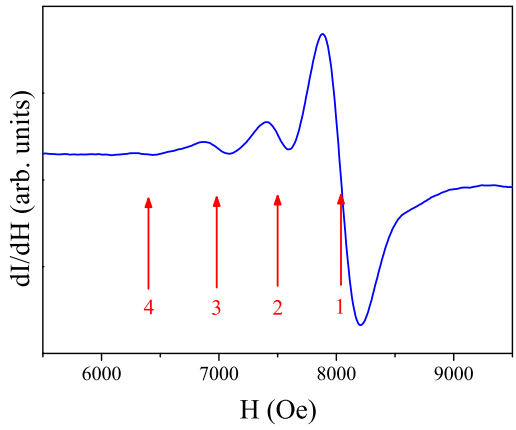

FIG. 2. The magnetic resonance spectrum of the nickel triangular dots array recorded at room temperature at 9.86 GHz. Magnetic field is perpendicular to the array plane. Resonance lines positions are denoted by arrows and the corresponding values of resonance fields are presented in Table I.

The magnetization precession in the linear approximation can be described as following: z component of the magnetization is constant and equal to the saturation magnetization while the time-dependent small component ($m \ll M_0$) is in xy plane, i.e., $\mathbf{M} = M_0\mathbf{e}_z + \mathbf{m}e^{i\omega t}$.

The magnetic free energy of the system can be presented as

$$F = \int_{V_p} \left[\frac{1}{2}\alpha(\nabla \mathbf{M})^2 - \mathbf{H}^0 \cdot \mathbf{M} - \frac{1}{2}\mathbf{H}^m \cdot \mathbf{M} - \frac{1}{2}\beta \mathbf{M}_z^2 \right] dV, \tag{1}$$

where the integration is performed over the pyramid volume V_p. The first term is the energy of inhomogeneous exchange, the second one is the Zeeman energy, the third one is energy of the dipole-dipole interaction, and the last term is the anisotropy energy. $\mathbf{H}^0$ is the external magnetic field, which is directed perpendicularly to the array plane; $\mathbf{H}^m$ is the demagnetizing the demagnetizing field, $\alpha = 2A/M_0^2$ is the exchange constant; A is the exchange stiffness constant.

The magnetic dynamics of the system can be described by Landau-Lifshitz (LL) equation:

$$\frac{d\mathbf{M}}{dt} = -\gamma[\mathbf{H}^{\text{eff}} \times \mathbf{M}], \tag{2}$$

where $\mathbf{H}^{\text{eff}} = -\frac{\delta F}{\delta \mathbf{M}}$ is the effective magnetic field and γ is the gyromagnetic ratio.

TABLE I. The comparison of the theoretically calculated resonance field values for SW modes with the experimental data.

Mode number j	H_j^0, Oe (experiment)	H_j^0, Oe (theory)	Main basis function
1	8040	8040	$\|101\rangle$
2	7500	7508	$\|201\rangle$
3	6980	7000	$\|211\rangle$
4	6400	6700	$\|301\rangle$

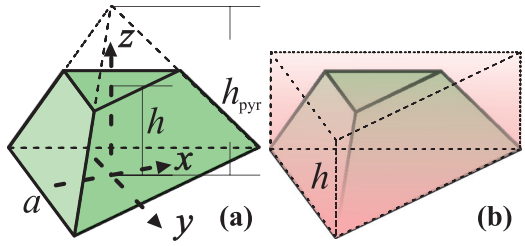

FIG. 3. (a) Coordinate system and its position with respect to the pyramid. Here, a is the base side of the truncated pyramid, h is its height, and h_{pyr} is the height of the corresponding nontruncated pyramid. (b) The sketch of prism and its transformation into the pyramid.

Taking into account (1) and (2) the following system of linearized LL equations can be obtained:

$$\begin{cases} i\omega m_x = \gamma\left[-\alpha M_0 \Delta m_y + \left(H^0 + H_z^m + H_A\right)m_y - M_0 h_y\right] \\ -i\omega m_y = \gamma\left[-\alpha M_0 \Delta m_x + \left(H^0 + H_z^m + H_A\right)m_x - M_0 h_x\right] \end{cases}, \tag{3}$$

where $\Delta = \frac{\partial^2}{\partial x^2} + \frac{\partial^2}{\partial y^2} + \frac{\partial^2}{\partial z^2}$ is the Laplacian in a Cartesian coordinate system, the z component of the static demagnetizing field is

$$H_z = -M_0 \frac{\partial}{\partial z} \int_{V_P} dV' \frac{\partial}{\partial z'} \frac{1}{|\mathbf{r} - \mathbf{r}'|}, \tag{3a}$$

and the planar components of the dynamic demagnetizing field are

$$h_\eta = -\frac{d}{d\eta} \int_{V_P} dV' (\mathbf{m} \cdot \nabla') \frac{1}{|\mathbf{r} - \mathbf{r}'|}, \quad \eta = x, y.$$

$H_A = \beta M_0$ is the magnetic anisotropy field.

In most cases it is impossible to obtain an exact analytical solution of LL equation for the SWs in nanostructures with strongly inhomogeneous demagnetizing fields. Usually the Ritz method is used to find approximate solutions [26]. These solutions can be chosen based on particle shape and magnetization boundary conditions.

In the earlier considered cases [7–14], the characteristic planar sizes of dots were mostly much larger than their thickness. As a result, the demagnetizing field is practically homogeneous throughout the volume of a dot. Variation of demagnetizing fields can be observed only near the dot borders.

For thin cylindrical dots the zero order Bessel functions of the first kind are good approximation to describe 2D standing SW profiles ("drum modes") [7]. A superposition of the Bessel functions of the first and the second kind were used to describe SW profiles in rings [14]. Trigonometric functions served for the description of SW profiles in rectangular dots and stripes (planar waves) [12,27]. In the case of triangular thin prism ($a \gg h$) the demagnetizing field is practically homogeneous throughout the volume and 2D standing wave profiles of a triangular medium (triangular membrane oscillations) eigenfunctions (see below) can be chosen as spin wave profiles.

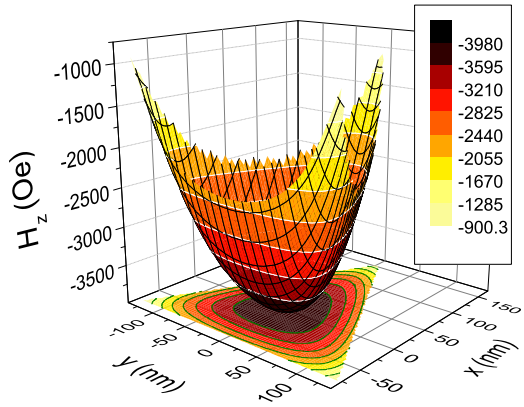

FIG. 4. The in-plane dependence of prism demagnetization field on xy plane calculated using (3a) with the following parameters: $a = 270$ nm, $h = 70$ nm, and $M_0 = 484$ emu/cm^3.

The situation in our truncated pyramids differs from the mentioned above. These pyramids cannot be considered as planar particles, because a and h are comparable. As a result, the distribution of the local demagnetizing fields is inhomogeneous throughout the pyramid volume. This inhomogeneity plays a role of potential well for SWs.

Unfortunately the height of the nontruncated pyramid h_{pyr} [see Fig. 3(a)] cannot be exactly evaluated from the AFM measurements. In the first approximation let the dots shape be prismoidal ($h \ll h_{\text{pyr}}$, here h is the height of the truncated pyramid, see Fig. 3). This results in substantial simplifications of the analytical calculations because of the almost homogeneous distribution of the demagnetizing field along the height. This allows separating spatial variables in the eigenmodes equation. It is worth to be noted that the analytical approach developed here for the right triangular prisms can be applied for arbitrary thick n-gonal right prisms (including cylinder).

A. Model of regular prism

The distribution of local demagnetizing field in regular triangular prism $H_z^m(x, y)$ was calculated using Eq. (3a) and presented in Fig. 4 for the nickel prism with the parameters which are close to that for prisms investigated in the experiment. In thin disks [7–11], rings [13,14], or rectangles [12] investigated previously, the demagnetizing field was proved to be homogeneous over dots plane, excluding small regions near edges. This gives a possibility to choose the Bessel functions (for round-shaped planar particles) or trigonometrical functions (for rectangular ones) as a good approximation for eigen-modes shape. However, this assumption about homogeneous demagnetizing field over the dot plane is not valid in our case. The calculated in-plane dependence of the local demagnetizing field (Fig. 4) can be approximated by symmetrical paraboloid. The calculation also showed that the local demagnetizing field practically does not change with height and can be considered as constant in z direction. This gives the possibility to apply an analytical approach, developed in [28] for spin waves in parabolic potential. H_z^m was approximated as

$$H_z^m = \left|H_z^{m(0)}\right|(-1 + C(x^2 + y^2)), \tag{4}$$

where $|H_z^{m(0)}|$ determines the depth of the well, C is a parameter of well curvature. For the considered prism the variation of a static demagnetization can be fitted using the following parameters: $H_z^{m(0)} = 4033\,\text{Oe}$ and $\text{C} = 5.3 \times 10^9\,\text{cm}^{-2}$.

Such behavior of the demagnetizing field is similar to the distribution of magnetic fields inside thin ferromagnetic film induced by magnetic sphere [28]. It has been shown [28] that LL equation for SWs in this case can be reduced to the system of coupled Schrödinger-like equations for quantum harmonic oscillator. Therefore, the wave function can be presented as a product of single-coordinate functions, which are proportional to Hermite polynomials for x and y coordinates and harmonic function for z. Strong pinning on the boundaries is assumed.

$$\Psi_{nml}(\mathbf{r}) = \varphi_n(Kx)\varphi_m(Ky)\phi_l(z), \tag{5}$$

where $\phi_l(z) = \sqrt{2/h}\sin(k_z l z)$, $k_z = \pi/h$, n , m , l are integer numbers; the value $K = (\frac{\text{C}|H_z^{m(0)}|}{\alpha M_0})^{1/4}$ has a dimension of a wave vector, $\varphi_i(u) = \frac{1}{\sqrt{2^i\sqrt{2\pi}}} H_i(u) e^{-\frac{u^2}{2}}$; $i = m, n$; $u = Kx, Ky$, m, n are the indexes of the mode, $H_i(u) = (-1)^i e^{\frac{u^2}{2}} \frac{d^i}{du^i} e^{-\frac{u^2}{2}}$ are the Hermite polynomials. K in $\varphi_m(Kx)$ and $\varphi_n(Ky)$ has the same value due to the symmetry of potential well in xy plane.

In such a case, $\Psi_{nml}(\mathbf{r})$ are the eigenfunctions of the Hamiltonian-like operator $\hat{\mathbf{H}}(\mathbf{r})$:

$$\hat{\mathbf{H}}(\mathbf{r})\Psi_{nml}(\mathbf{r}) \equiv (-\Delta + K^4(x^2 + y^2))\Psi_{nml}(\mathbf{r}) = \varepsilon_{nml}\Psi_{nml}(\mathbf{r})$$

where $\varepsilon_{nml} = [(2n+1) + (2m+1)]K^2 + k_z^2 l^2$ are its eigenvalues. This is valid only for the low-energy levels with the corresponding wave functions localized inside the prism boundaries.

Neglecting h_x and h_y terms in (3) exact solutions of the LL equation can be obtained. The corresponding SW modes can be considered as independent.

A diagonal approximation is used here for the theoretical explanation of SW resonances in triangle prisms, like it was done before in Refs. [9,11,28]. Without the integrodifferential terms h_x, h_y in (3), the set of orthogonal functions (5) can be an exact solution of the equations (3) with the demagnetizing field (4). In this case, modes with different indices are not coupled. The existence of the dynamic dipolar field h_x, h_y leads to the interaction between modes with different indices. To avoid this problem, the diagonal approximation, developed in [9,11,28] was used as a first approximation. This approximation is based on the supposition of small values of nondiagonal terms of the dynamic dipolar operator in comparison with diagonal ones. Our numerical calculations have shown this is valid for the prismoidal shape dots. According to Eqs. (3)–(5), the matrix representation of corresponding operator in this case has a simple diagonal form with corresponding allowed set of localized standing modes and eigenvalues.

In the diagonal approximation, the dispersion relation takes the form:

$$\omega_{nml} = \gamma\sqrt{(H^0 + H_{nml} - \langle h_x\rangle_{nml})(H^0 + H_{nml} - \langle h_y\rangle_{nml})}, \tag{6}$$

where $H_{nml} = \alpha M_0 \varepsilon_{nml} + H_A - |H_z^{m(0)}|$ and resonance field H^0 at fixed frequency is

$$H^0 = -H_{nml} + \frac{\langle h_x + h_y\rangle_{nml}}{2} + \sqrt{\frac{\omega_{nml}^2}{\gamma^2} + \frac{\langle h_x - h_y\rangle_{nml}^2}{4}}.$$

Here, $\langle h_x\rangle_{nml}$ and $\langle h_y\rangle_{nml}$ are

$$\langle h_\eta\rangle_{nml} = -M_0 \int_{V_P} dV \int_{V_P} dV' \Psi_{nml}(\mathbf{r})\Psi_{nml}(\mathbf{r}') \times \frac{d^2}{dr_\eta dr'_\eta}\frac{1}{|\mathbf{r} - \mathbf{r}'|}. \tag{7}$$

The following parameters were used for numerical calculations of SW resonance fields: $M_0 = 484\,\text{Oe}$, $A = 8 \times 10^{-7}\,\text{erg/cm}$, $K = 2.6 \times 10^5\,\text{cm}^{-1}$, and $f = 9.86\,\text{GHz}$. The saturation magnetization M_0 and the exchange stiffness constant A values are typical for Ni. Resonance frequency value f is the same as in the experiment. The magnetic anisotropy constant K was used as a parameter to fit the position of the most intensive resonance line. In our case this parameter does not effect on the distances between peaks but shifts the position of the spectrum.

Profiles of the modes with odd indexes m and n are antisymmetrical and these SWs cannot be registered using FMR technique, because of zero amplitude of the corresponding resonance signals. Only the modes with even indexes m and n can be experimentally observed. It should be noted that these modes could be observed in the experiment on Brillouin light scattering, but there are technical problems for the application of this technique for the investigation of the standing spin waves in the studied structures. The modes with the smallest indexes having highest intensity, namely $|001\rangle$, $|201\rangle$, and $|221\rangle$ should be observed in the experiment. It should be noted that the profile of the second resonance mode is symmetrical with respect to x and y and as a result, it is doubly degenerated (indexes $|201\rangle$ and $|021\rangle$). These spectrum lines are practically equidistant as it is observed in the experiment. The calculated interval between the resonance lines of the corresponding modes is of about 1200 Oe. It should be noted that described analytical approach could be used for wide variety of dot shapes where demagnetizing field dependence on plane coordinates could be approximated with paraboloid. However, the distances between resonance peaks obtained in the frame of the prism shape model are twice larger than in the experiment. This discrepancy is related to the fact that nickel islands are not prisms. The shape of islands can be better approximated by truncated pyramid shape (frustrum).

B. Model of truncated pyramid

In truncated pyramid the in-plane dependence of the local demagnetizing field $H_z^m(x, y)$ dramatically changes with the height z, nevertheless its shape is close to paraboloid. In the case of truncated pyramid, it is impossible to separate the variables in (3). One of the most straightforward way to overcome this problem is to use the quantum-mechanical variational method approach: displacing boundaries of prism to obtain frustrum [see Fig. 3(b)]. Taking the height of nontruncated pyramid h_{pyr} as a free parameter the best correlation with the

experiment can be obtained for $h_{\rm pyr} = 2h$. However, in this case, only one energy level is located inside parabolic potential. All other modes are above the paraboloid potential and confined by triangular well boundaries. The eigenfunctions of a quantum oscillator in this case are not already a good set to describing the eigenmodes of frustrum due to strong variation of demagnetizing field with height. Therefore the orthogonal set of the 2D standing wave profiles of a triangular medium [29], instead of Hermitian functions, was used as the basis:

$$\Psi^{(\rm pr)}_{nml}(\mathbf{r}) = A_m \psi^{(\rm tr)}_{nm}(x,y)\phi_l(z), \tag{8}$$

where $\phi_l(z) = \sqrt{2/h}\sin(\pi l z/h)$ and $\psi^{(\rm tr)}_{nm} = \sin[(n-m)k_x x_c]\cos[(m+n)k_y y] + \sin[(2m+n)k_x x_c]\cos[nk_y y] - \sin[(2n+m)k_x x_c]\cos[mk_y y]$, $n > m$, $x_c = x - a/\sqrt{3}$, $k_x = 2\pi/a\sqrt{3}$ and $k_y = 2\pi/a$.

$A_m = 4(3\sqrt{3}a^2(1+\delta_{m0}))^{-1/2}$ is the normalization constant, δ_{nm} is the Kronecker delta. Corresponding Laplace operator eigenvalues for these functions are

$$-\Delta_{x,y}\psi_{nm}(x,y) = 4k_x^2(n^2+m^2+nm)\psi_{nm}(x,y).$$

SW eigenmodes in frustrum can be expanded into the "prismoidal" SW basis: $\Psi^{(\rm pyr)} = \sum C^{\alpha}_{nml}\Psi^{(\rm pr)}_{nml}$ and dynamical magnetization components take form:

$$m_x = \sum_{\mathbf{n}} X_{\mathbf{n}}\Psi^{(\rm pr)}_{\mathbf{n}}, \quad m_y = \sum_{\mathbf{n}} Y_{\mathbf{n}}\Psi^{(\rm pr)}_{\mathbf{n}},$$

where for brevity $\mathbf{n} = (n, m, l)$. The diagonal approximation (6) for frustrum would be too rough because $\Psi^{(\rm pr)}_{\mathbf{n}}$ functions are the eigenfunctions only for the Laplacian disregarding a coordinate dependence of the demagnetizing field $H^m_z(\mathbf{r})$. Taking into consideration prismoidal modes interaction, (3) is reduced to standard eigenvalues equation:

$$-(H^0 + H_A)\begin{pmatrix} X_{\mathbf{n}} \\ Y_{\mathbf{n}} \end{pmatrix} = \sum_{\mathbf{m}} \begin{pmatrix} E_{\mathbf{n}}\delta_{\mathbf{nm}} + \langle H^m_z\rangle_{\mathbf{nm}} - \langle h_x\rangle_{\mathbf{nm}} & -i\frac{\omega}{\gamma}\delta_{\mathbf{nm}} \\ i\frac{\omega}{\gamma}\delta_{\mathbf{nm}} & E_{\mathbf{n}}\delta_{\mathbf{nm}} + \langle H^m_z\rangle_{\mathbf{nm}} - \langle h_y\rangle_{\mathbf{nm}} \end{pmatrix}\begin{pmatrix} X_{\mathbf{m}} \\ Y_{\mathbf{m}} \end{pmatrix}, \tag{9}$$

where $E_{\mathbf{n}} = \alpha M_0(4k_x^2(n^2+m^2+nm) + (\frac{\pi l}{h})^2)$, $\langle H^m_z\rangle_{\mathbf{nm}} = \int_{V_{\rm pyr}} dV \Psi^{(\rm pr)}_{\mathbf{n}}(\mathbf{r}) H^m_z(\mathbf{r}) \Psi^{(\rm pr)}_{\mathbf{m}}(\mathbf{r})$, and $\langle h_{x(y)}\rangle_{\mathbf{nm}}$ are calculated using (7), where integration over the frustrum volume is performed. A truncated basis set of triangular eigenfunctions (8) with lowest eigenvalues $\{\Psi^{(\rm pr)}_{101}, \Psi^{(\rm pr)}_{201}, \Psi^{(\rm pr)}_{211}, \Psi^{(\rm pr)}_{301}, \Psi^{(\rm pr)}_{311}, \Psi^{(\rm pr)}_{321}, \Psi^{(\rm pr)}_{401}, \Psi^{(\rm pr)}_{411}, \Psi^{(\rm pr)}_{421}$ and $\Psi^{(\rm pr)}_{501}\}$ was chosen to describe the resonances observed in the experiment. The corresponding matrix (9) is strictly diagonally dominant matrix where the fourth diagonal element values already does not exceed 2% of the corresponding main diagonal element values. According to Gershgorin circle theorem the matrix eigenvalue deviation from diagonal value does not exceed the sum of the absolute values of the nondiagonal entries in this row: $|\lambda_i - H_{ii}| < \sum_{j\neq i}|H_{ij}|$. Therefore, even for the first six eigenfunctions from the truncated basis set, the error in the determination of the corresponding eigenvalues does not exceed 5%.

For the prism ($h/h_{\rm pyr} \to 0$), only triangular eigenmodes with index $m = 0$ have nonzero net amplitudes and can be experimentally observed using FMR technique (see Appendix for the details):

$$I_{nm} \sim \left(\int \psi^{(\rm tr)}_{nm}(x,y)dxdy\right)^2 = \frac{3^{3/2}}{2}\left(\frac{a}{\pi n}\right)^2\delta_{m0}. \tag{10}$$

All modes with observed intensity have the symmetry of an equilateral triangle (Fig. 5).

Strictly speaking, Eq. (10) is valid for the prism but cannot be applied for the frustrum. Transition to the frustrum results in a decrease of system symmetry and previously nonvisible modes can be observed. As an example to demonstrate this, let us consider mode $|211\rangle$. The profile of this mode is presented in Fig. 5(a). Unperturbed mode (prismoidal) has seven extrema. The oscillations taking place in three regions situated near the triangle sides compensate antiphase oscillations in four others regions in the vicinity of the triangle center and corners. Because planar prismoidal wave function $\psi^{(\rm tr)}_{nm}(x,y)$ does not depend on z then its net intensity is equal to zero. But the profile of corresponding frustrum mode is changing with height and as a result this mode has nonzero net intensity. For example, only one extremum of magnetic oscillations amplitude of $|211\rangle$ can appear near the frustrum top base, like it was shown in Ref. [30]. The similar effect should be observed here [see Fig. 5(b)].

Our calculations show that for chosen parameters the $|301\rangle$ mode eigenvalue E_{301} is close to E_{102} of $|102\rangle$ mode. Because this mode is altering with the height and due to its strong in-plane localization it cannot be observed both in prism and frustrum cases.

Therefore the frustrum spectrum is mainly determined by "prismoidal" SW $|101\rangle$, $|201\rangle$, $|211\rangle$, and $|301\rangle$. However, in the case of frustrum, there is a substantial admixture of neighboring states. It should also be pointed out that $|211\rangle$ mode can be observed by FMR for a frustrum but cannot be observed for a prism.

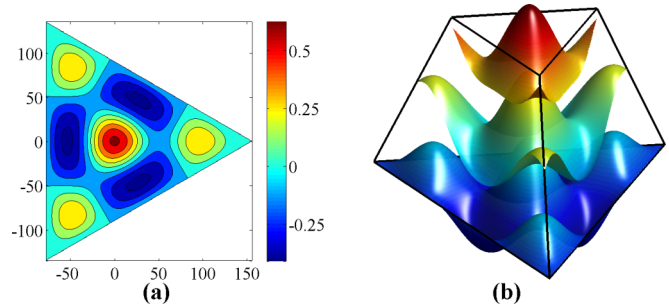

FIG. 5. The triangular membrane oscillations eigenfunction $\psi^{(\rm tr)}_{21}$ profile (a) calculated using (8) with the parameters described in the text. Bright and dark colors correspond to the areas oscillating in antiphase. (b) The same eigenfunction profiles for heights $z = 0, h/2, h$ in truncated pyramid.

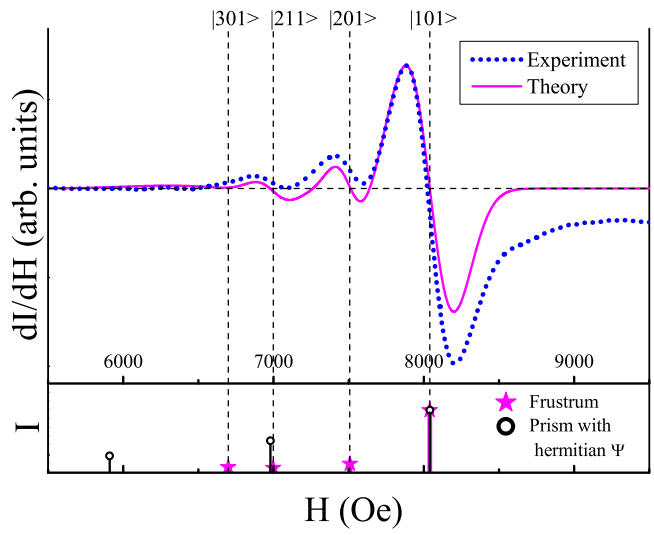

FIG. 6. Magnetic resonance spectrum of nickel dots: the experiment (dotted line) and the theory for frustrum (solid line). Theoretical lines positions (see bottom inset) for the cases of regular prisms (circles) and frustrums (stars) were obtained solving Eqs. (6) and (9) correspondingly. The intensities of the lines were calculated using standard approach $I_j \sim (\int \Psi_j dV)^2$. The theoretical spectrum was plotted in supposition of Gaussian shape of the lines. The dispersion was evaluated from the experiment.

The comparison of experimental and theoretical (calculated for frustrum) resonance fields is presented in Table I. The following parameters were used for the calculations: $M_0 = 484$ Oe, $A = 8 \times 10^{-7}$ Erg/cm, $\gamma = 1.82 \times 10^7$ s^{-1} Oe^{-1}, and $f = \omega/2\pi = 9.86$ GHz.

The distances between resonance lines are determined by static and dynamic demagnetizing fields and exchange field calculated above, while lines position strongly depends on H_A. Best fit of the experimental data was obtained using $H_A = \beta M_0$, where $\beta = -5.8$, i.e., in supposition that there is an easy plane magnetic anisotropy in nickel dots. Usually tensile stresses in nickel films result in the formation of perpendicular to the film plane uniaxial anisotropy. However, the investigated nickel dots were grown on 111 Si single crystal substrate which results to their compression stresses. This statement (tensile stresses on the silicon substrate surface and corresponding compressive stresses in Ni dots) is confirmed by the experiments on surface phonon propagation in such structure [31].

Obtained analytical results (see Fig. 6) are in good agreement with experimental data. However proposed theoretical approach can be improved considering next nonlinear terms in Eq. (2) [32] or by more delicate analysis of integrodifferential LL equations (3) [33].

IV. SUMMARY

Standing spin waves in triangular dots in perpendicular saturating magnetic field have been investigated both experimentally and theoretically. Four resonance modes were observed in the experiment. Although these modes are quite similar to that observed before for thin magnetic submicron dots of different shapes (circular, rectangular, etc.), the well developed theoretical approach [7–11,14] cannot be applied for our case because of strong lateral variation of the demagnetizing fields. First it has been assumed that the geometrical shape of dots is a prismoidal. Then the variation of the demagnetizing fields can be approximated by paraboloid function and SW mode with lowest energy can be presented as ground state eigenmode of two-dimensional harmonic oscillator. The upper energy modes have been taken as triangular membrane eigenmodes. It should be noted that the developed theoretical approach can be applied for magnetic particles of n-gonal right prism shapes (including cylinder) where the aspect ratio is not negligibly small and a spatial dependence of a demagnetizing field cannot be neglected. But in this approximation the theoretical intervals between resonance fields are twice larger then experimentally observed. To improve the correlation between the theory and experiment it has been taken into account that the real shape of dots is closer to truncated pyramids. SW eigenmodes in frustrum was obtained as the superposition of prismoidal eigenfunctions taking into consideration the intermodes interaction in the frame of the quantum mechanical variational method. This allows to achieve perfect agreement between the theory and experiment.

ACKNOWLEDGMENTS

The authors thank Mateusz Zelent and Boris A. Ivanov for stimulating discussions. The research leading to these results has received funding from the European Union Horizon 2020 research and innovation program under Marie Sklodowska-Curie Grant Agreement No. 644348 (MagIC) and from the Polish National Science Centre Project No. UMO-2016/21/B/ST3/00452. This work was partially supported by Nanoscience and Nanotechnology Grant 1/19-H provided by National Academy of Sciences of Ukraine. J.K. and P.B. are grateful for the support from Grant 23-04/01-2019 for young scientists of National Academy of Sciences of Ukraine.

APPENDIX

According to Ref. [29], the 2D standing wave profiles of a triangular medium are

$$\begin{aligned}\psi_{nm}^{(\mathrm{tr})}/A_m = {} & \sin[(n-m)k_x x]\cos[(m+n)k_y y] \\ & + \sin[(2m+n)k_x x]\cos[nk_y y] \\ & - \sin[(2n+m)k_x x]\cos[mk_y y], \end{aligned} \tag{A1}$$

where $n > m \geqslant 0$, $k_x = 2\pi/a\sqrt{3}$, and $k_y = 2\pi/a$; $A_m = 4(3\sqrt{3}a^2(1+\delta_{m0}))^{-1/2}$ is the normalization constant; δ_{nm} is the Kronecker delta; $x = a\sqrt{3}/2$ and $y = \pm x/\sqrt{3}$ are the side lengths of the triangular prism cross-section.

The resonance signal intensity for the corresponding eigenmodes is proportional to the integrated eigenfunction profile:

$$I_{nm} \sim \left(\int \psi_{nm}^{(\mathrm{tr})}(x,y)dxdy\right)^2 = A_m^2\left(\int_0^a dx\left(\int_{-x/\sqrt{3}}^{x/\sqrt{3}} \psi_{nm}^{(\mathrm{tr})}(x,y)dy\right)\right)^2.$$

The integral over the cross-sectional area for sine and cosine products in (A1) can be reduced to

$$\begin{aligned}\int_0^{a\sqrt{3}/2} dx\sin(\beta k_x x)\int_{-x/\sqrt{3}}^{x/\sqrt{3}}\cos(\alpha k_x\sqrt{3}y)dy &= \frac{2}{\alpha k_x\sqrt{3}}\int_0^{a\sqrt{3}/2}\sin(\beta k_x x)\sin(\alpha k_x x)dx\\ &= \frac{1}{\alpha k_x\sqrt{3}}\int_0^{a\sqrt{3}/2}(\cos(\alpha-\beta)k_x x-\cos(\alpha+\beta)k_x x)dx\\ &= \frac{1}{\alpha k_x^2\sqrt{3}}\left(\frac{\sin(\alpha-\beta)\pi}{\alpha-\beta}-\frac{\sin(\alpha+\beta)\pi}{\alpha+\beta}\right),\end{aligned}$$

and this expression for integer α and β is nonzero only when $\alpha \pm \beta = 0$. For positive n and nonnegative m, this takes place only if $m = 0$. Thus for $|n0\rangle$ functions:

$$I_{n0} \sim A_0^2\left(\int [2\sin(nk_x x)\cos(nk_y y)-\sin(2nk_x x)]dxdy\right)^2 = A_0^2\left(\frac{\sqrt{3}\pi}{k_x^2 n}\right)^2 = \frac{3^{3/2}}{2}\left(\frac{a}{\pi n}\right)^2.$$

[1] S. Tehrani, E. Chen, M. Durlam, M. DeHerrera, J. M. Slaughter, J. Shi, and G. Kerszykowski, J. Appl. Phys. **85**, 5822 (1999).

[2] M. M. Miller, G. A. Prinz, S.-F. Cheng, and S. Bounnak, Appl. Phys. Lett. **81**, 2211 (2002).

[3] J. Ding, M. Kostylev, and A. O. Adeyeye, Appl. Phys. Lett. **100**, 073114 (2012).

[4] V. V. Kruglyak, S. O. Demokritov, and D. Grundler, J. Phys. D **43**, 264001 (2010).

[5] *Magnonics: From Fundamentals to Applications*, edited by S. O. Demokritov and A. N. Slavin (Springer, Berlin, 2013).

[6] P. Gruszecki and M. Krawczyk, in *Wiley Encyclopedia of Electrical and Electronics Engineering*, edited by J. G. Webster (Wiley, Hoboken, 2016), pp. 1–23.

[7] G. N. Kakazei, P. E. Wigen, K. Yu. Guslienko, V. Novosad, A. N. Slavin, V. O. Golub, N. A. Lesnik, and Y. Otani, Appl. Phys. Lett. **85**, 443 (2004).

[8] G. N. Kakazei, G. R. Aranda, S. A. Bunyaev, V. O. Golub, E. V. Tartakovskaya, A. V. Chumak, A. A. Serga, B. Hillebrands, and K. Y. Guslienko, Phys. Rev. B **86**, 054419 (2012).

[9] S. A. Bunyaev, V. O. Golub, O. Yu. Salyuk, E. V. Tartakovskaya, N. M. Santos, A. A. Timopheev, N. A. Sobolev, A. A. Serga, A. V. Chumak, B. Hillebrands, and G. N. Kakazei, Sci. Rep. **5**, 18480 (2016).

[10] O. Klein, G. de Loubens, V. V. Naletov, F. Boust, T. Guillet, H. Hurdequint, A. Leksikov, A. N. Slavin, V. S. Tiberkevich, and N. Vukadinovic, Phys. Rev. B **78**, 144410 (2008).

[11] K. Yu. Guslienko and A. N. Slavin, J. Appl. Phys. **87**, 6337 (2000).

[12] C. Bayer, J. Jorzick, B. Hillebrands, S. O. Demokritov, R. Kouba, R. Bozinoski, A. N. Slavin, K. Y. Guslienko, D. V. Berkov, N. L. Gorn, and M. P. Kostylev, Phys. Rev. B **72**, 064427 (2005).

[13] X. Zhou, J. Ding, M. Kostylev, and A. O. Adeyeye, Appl. Phys. Lett. **106**, 112403 (2015).

[14] X. Zhou, E. V. Tartakovskaya, G. N. Kakazei, and A. O. Adeyeye, Phys. Rev. B **96**, 024446 (2017).

[15] M. Miyata, K. Kiseki, S. Yakata, H. Wada, and T. Kimura, J. Appl. Phys. **111**, 07B902 (2012).

[16] X. Fu, S. D. Pollard, B. Chen, B.-K. Yoo, H. Yang, and Y. Zhu, Sci. Adv. **4**, eaat3077 (2018).

[17] M. Jaafar, R. Yanes, D. Perez de Lara, O. Chubykalo-Fesenko, A. Asenjo, E. M. Gonzalez, J. V. Anguita, M. Vazquez, and J. L. Vicent, Phys. Rev. B **81**, 054439 (2010).

[18] A. Vogel, A. Corinna Niemann, C. Stenner, A. Drews, M.-Y. Im, P. Fischer, and G. Meier, J. Appl. Phys. **112**, 063916 (2012).

[19] B. A. Ivanov and C. E. Zaspel, Appl. Phys. Lett. **81**, 1261 (2002).

[20] S. Yakata, T. Tanaka, K. Kiseki, K. Matsuyama, and T. Kimura, Sci. Rep. **3**, 3567 (2013).

[21] F. Montoncello and F. Nizzoli, J. Appl. Phys. **107**, 023906 (2010).

[22] A. Lara, V. Metlushko, M. García-Hernández, and F. G. Aliev, SPIN **04**, 1440003 (2014).

[23] A. Lara, J. Robledo Moreno, K. Y. Guslienko, and F. G. Aliev, Sci. Rep. **7**, 5597 (2017).

[24] J. Rybczynski, U. Ebels, and M. Giersig, Colloids and Surfaces A: Physicochem. Eng. Aspects **219**, 1 (2003).

[25] Z. P. Huang, D. L. Carnahan, J. Rybczynski, M. Giersig, M. Sennett, D. Z. Wang, J. G. Wen, K. Kempa, and Z. F. Rena, Appl. Phys. Lett. **82**, 460 (2003).

[26] L. D. Landau and E. M. Lifshitz, *Quantum Mechanics: Non-Relativistic Theory*, Course of Theoretical Physics Vol. 3 (Elsevier, Oxford, 2013).

[27] K. L. Livesey, J. Ding, N. R. Anderson, R. E. Camley, A. O. Adeyeye, M. P. Kostylev, and S. Samarin, Phys. Rev. B **87**, 064424 (2013).

[28] E. V. Tartakovskaya, M. Pardavi-Horvath, and R. D. McMichael, Phys. Rev. B **93**, 214436 (2016).

[29] B. R. Seth, Proc.: Math. Sci. **12**, 487 (1940).

[30] V. Lozovski and V. Piatnytsia, J. Comput. Theor. Nanos. **8**, 2335 (2011).

[31] A. Trzaskowska, S. Mielcarek, B. Graczykowski, B. Mroz, P. Patoka, and M. Giersig, J. Alloys Compd. **527**, 96 (2012).

[32] V. G. Bar'yakhtar and B. A. Ivanov, Zh. Exp. Teor. Fiz. **72**, 1504 (1977).

[33] E. B. Sonin, Phys. Rev. B **95**, 144432 (2017).